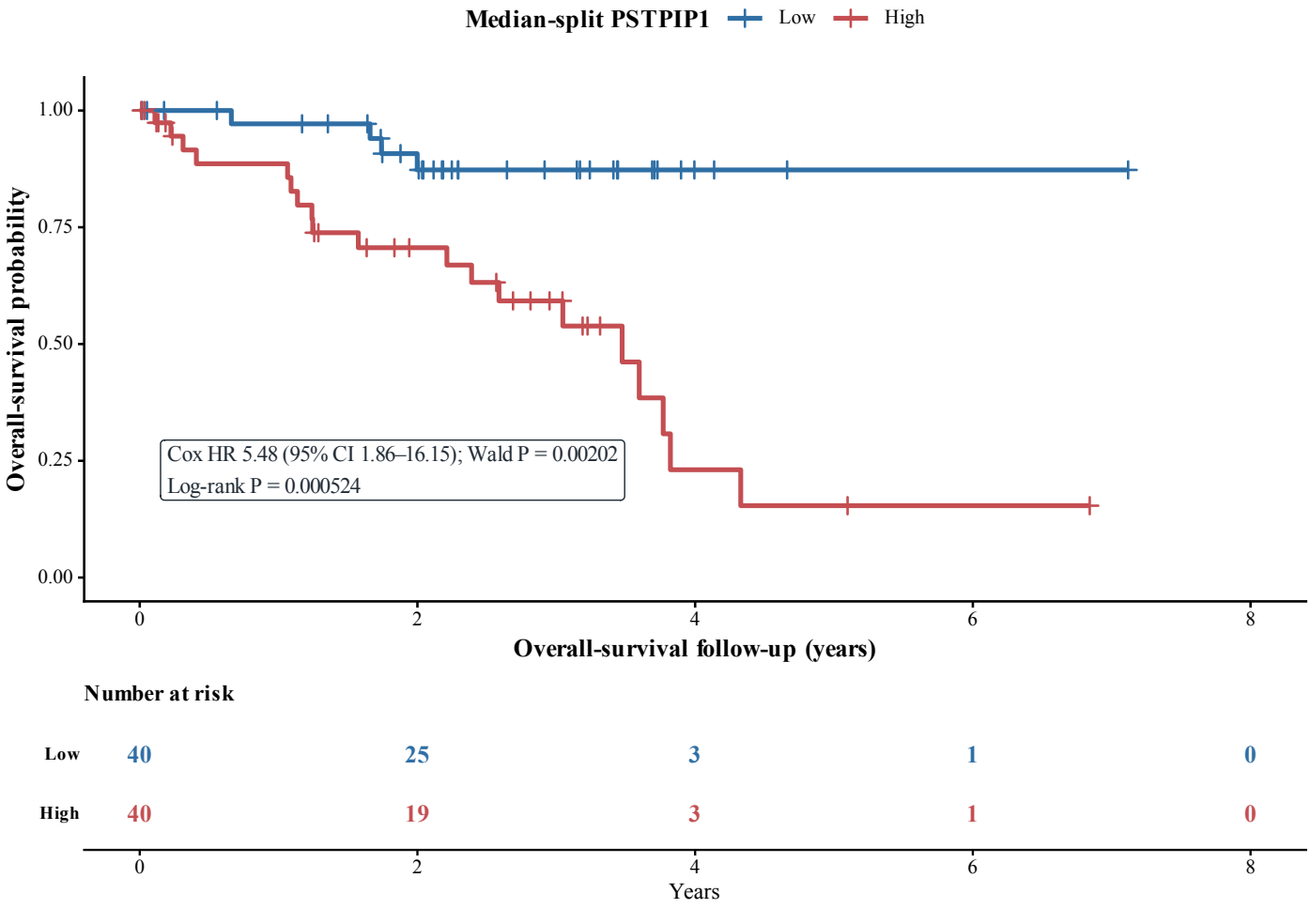
# Figure S1

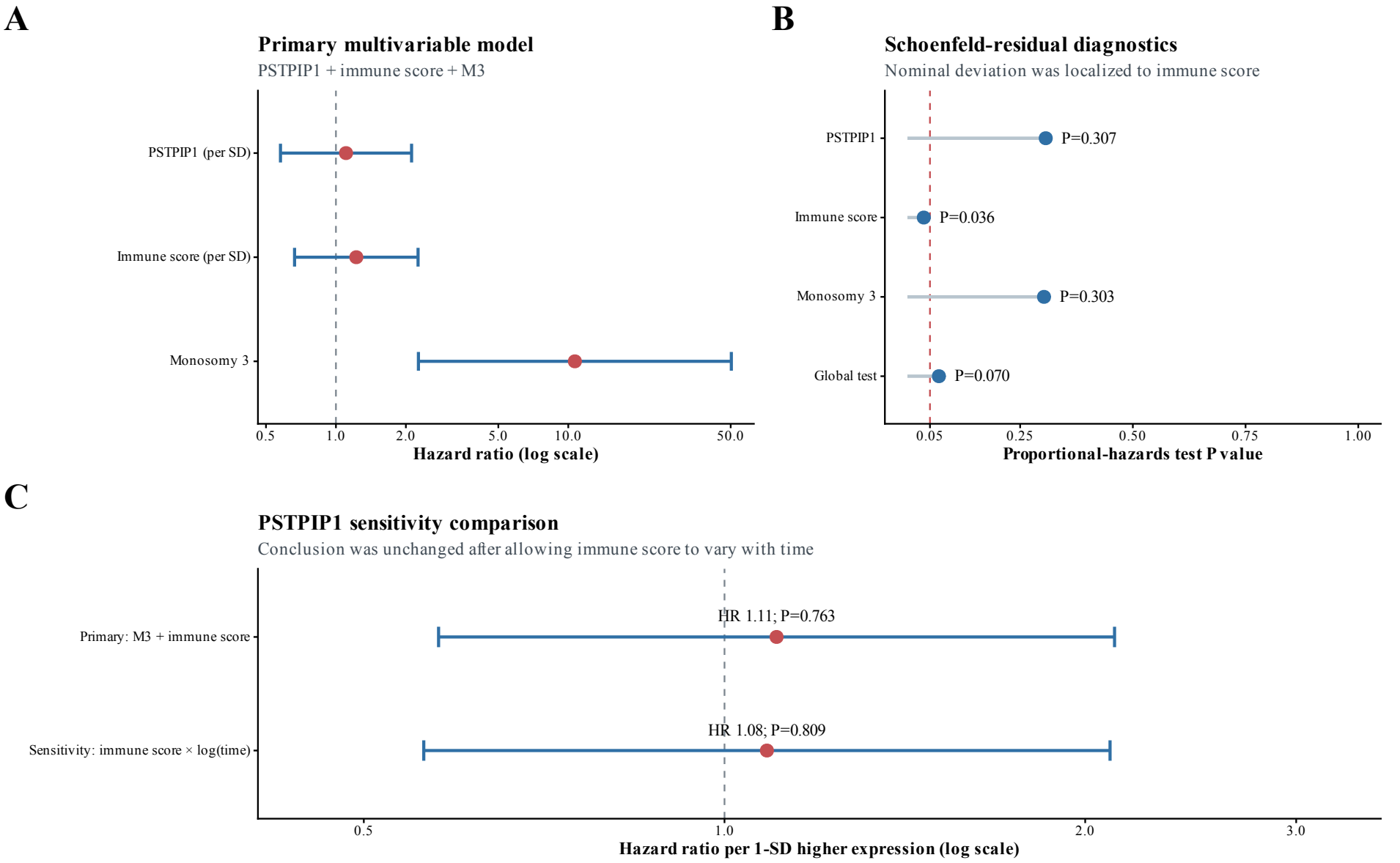
PSTPIP1 median-split overall survival in TCGA-UVM. The median split is a secondary descriptive analysis; continuous multivariable Cox models are the inferential analyses.




TCGA-UVM: n=80, 23 deaths; median PSTPIP1 expression = 1.017 log2(TPM+1). No outcome-optimized cutoff was used.

# Figure S2

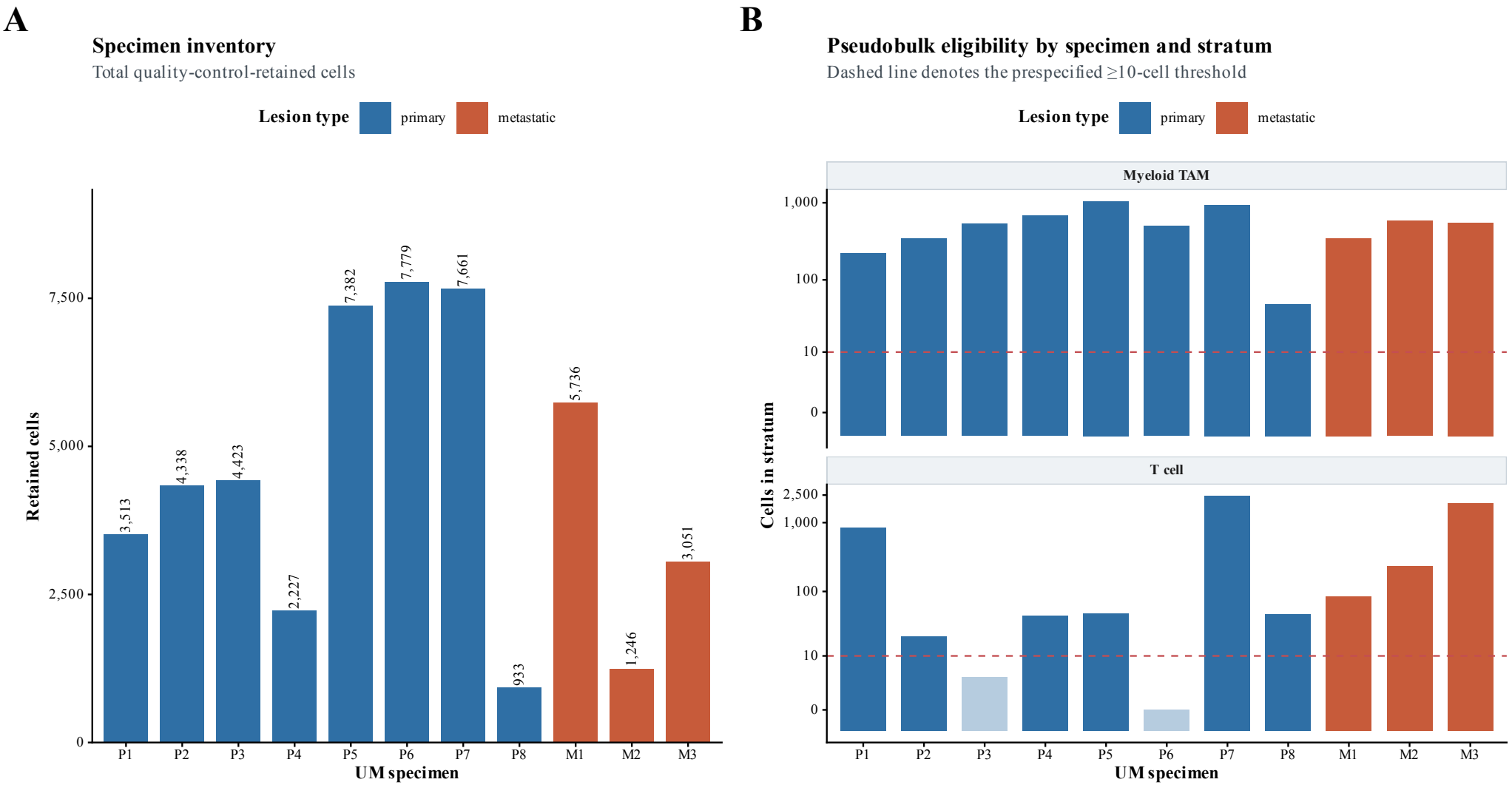
PSTPIP1 multivariable Cox model diagnostics and sensitivity analysis. TCGA-UVM: n=80 and 23 overall-survival deaths; the gene effect is standardized per 1-SD higher expression.




The primary model showed no independent PSTPIP1 association after immune score and M3 were included. Because the immune-score term showed a nominal PH deviation, a prespecified time-varying-coefficient sensitivity model was evaluated.

# Figure S3

Specimen inventory and pseudobulk eligibility in GSE139829. The dataset contained 48,289 cells from 11 specimens (8 primary and 3 metastatic UM).

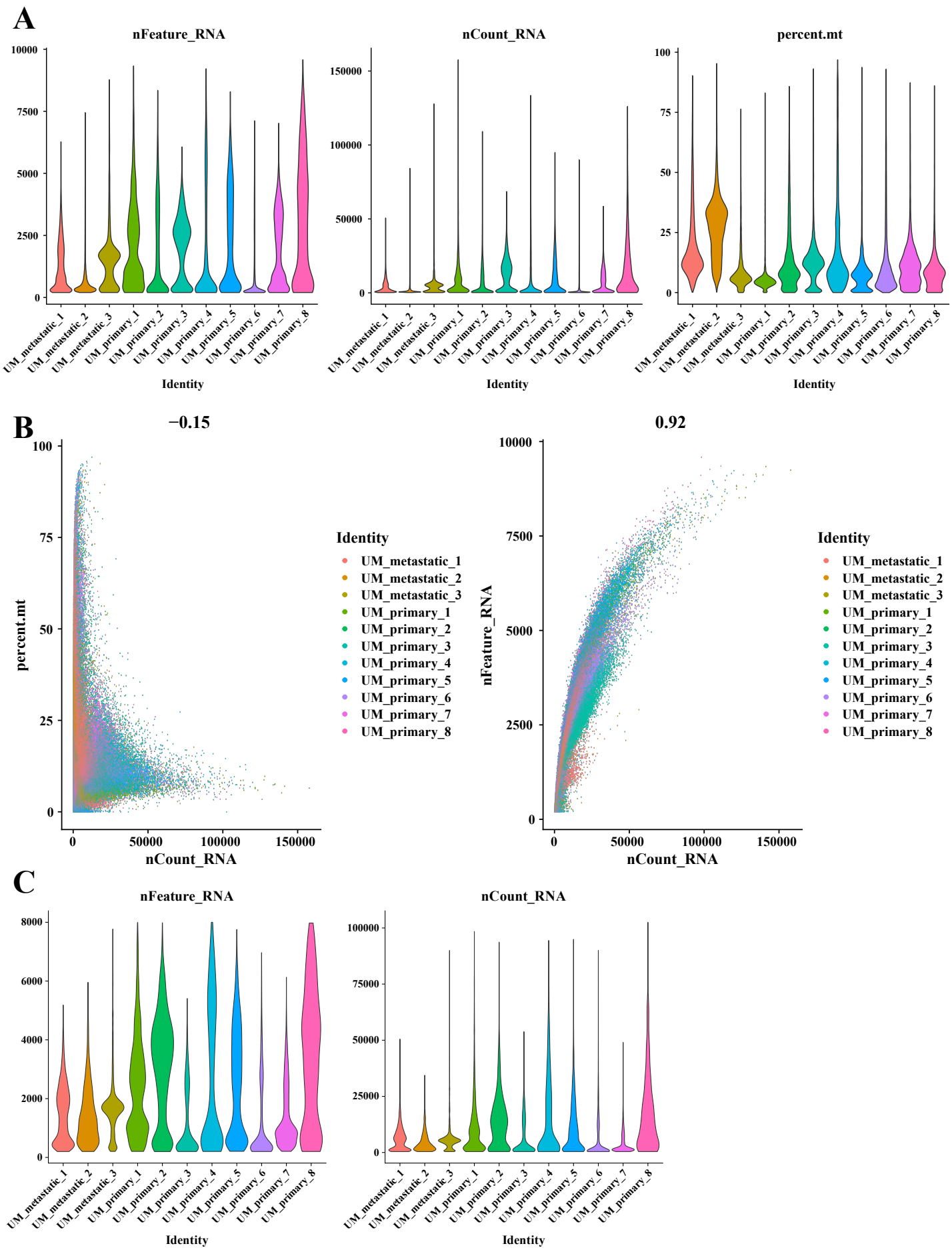



P, primary specimen; M, metastatic-lesion specimen. Myeloid/TAM analysis included 8 primary and 3 metastatic specimens; T-cell analysis included 6 primary and 3 metastatic specimens. The specimen—not the cell—was the inferential unit.

# Figure S4

**Single-cell RNA-seq quality control and global clustering of GSE139829.**

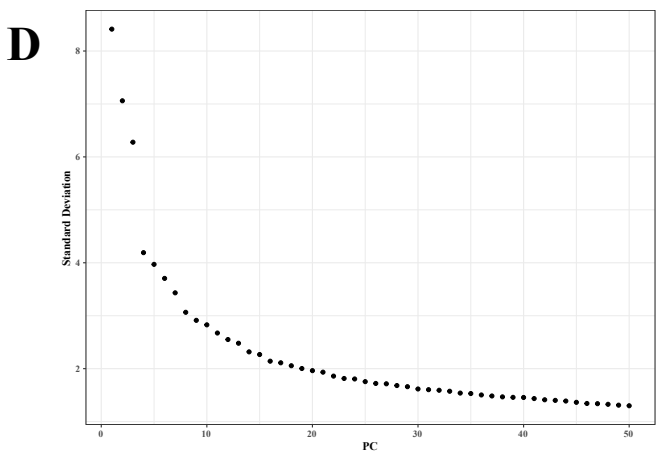
(A) Per-sample violin plots of nFeature_RNA, nCount_RNA, and percent.mt before filtering. (B) Scatter plots of percent.mt and nFeature_RNA against nCount_RNA with sample-wise correlation annotations. (C) Post-filter per-sample distributions of nFeature_RNA and nCount_RNA. (D) PCA standard-deviation elbow plot used to select the number of principal components. (E-F) Global Louvain clustering shown on t-SNE (E) and UMAP (F) embeddings. (G) Dot plot of canonical cell-type markers across clusters. (H) Feature plots for individual marker genes used for annotation. (I) Stacked violin plot of canonical markers across clusters.

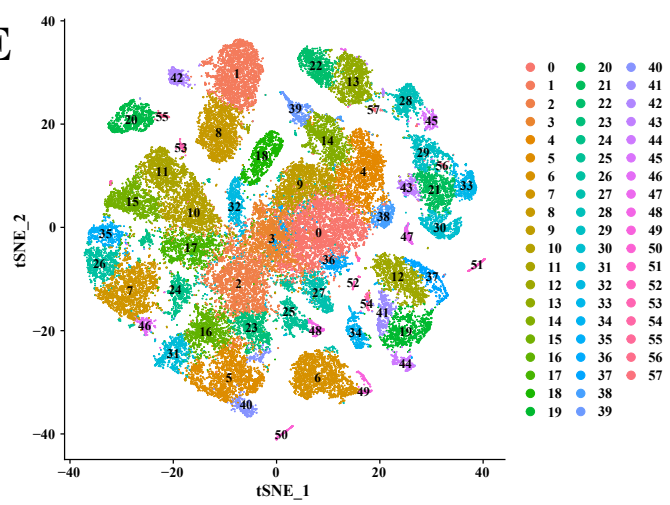


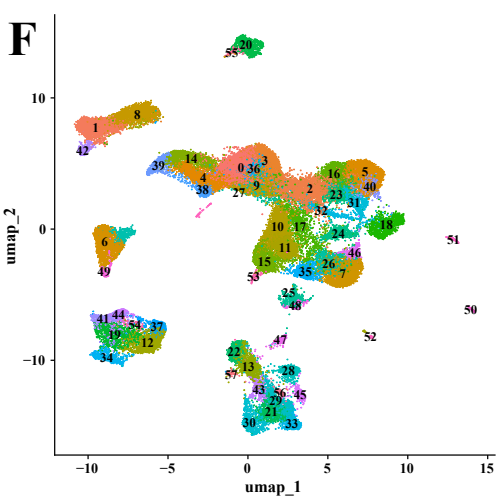
# Figure S4 (continued)

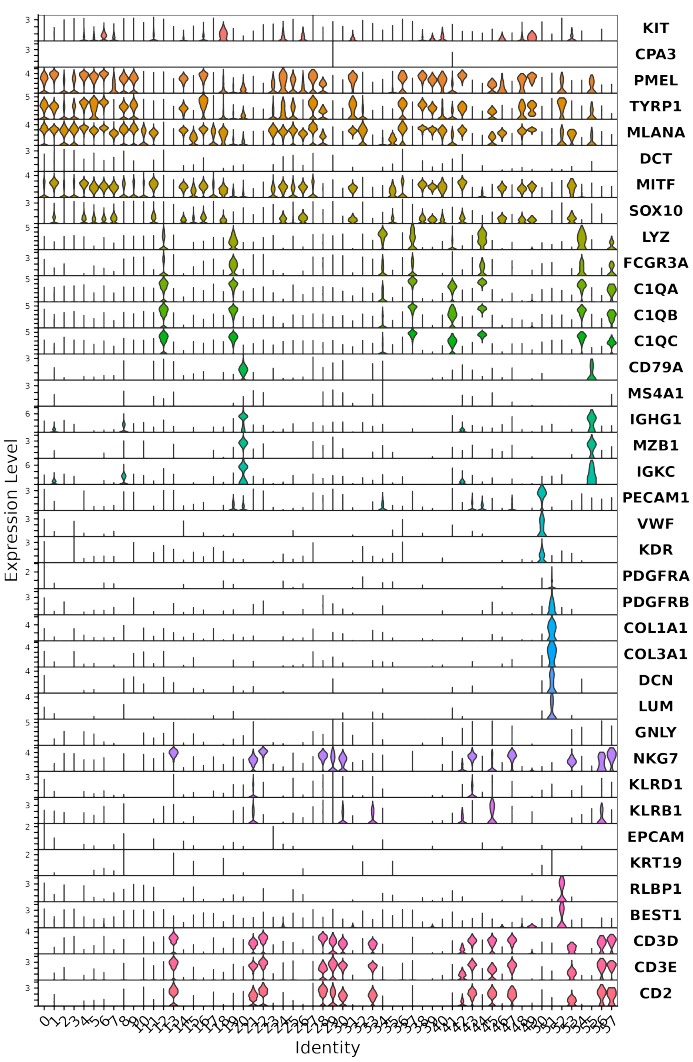
**Single-cell RNA-seq quality control and global clustering of GSE139829.**

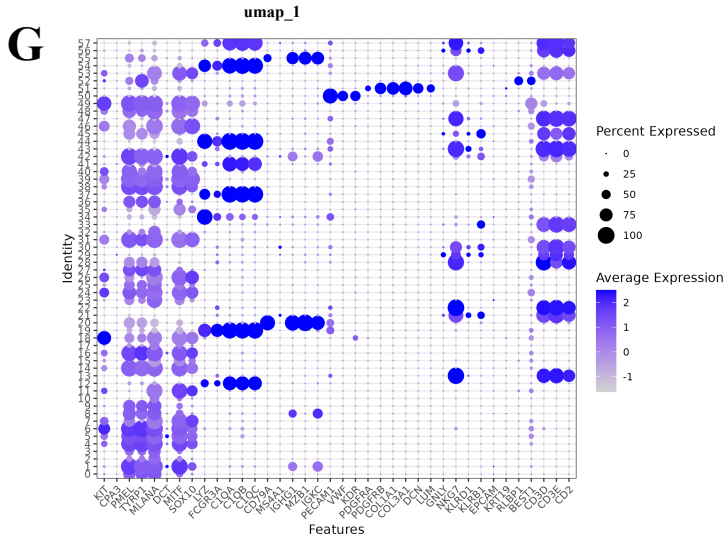
(A) Per-sample violin plots of nFeature_RNA, nCount_RNA, and percent.mt before filtering. (B) Scatter plots of percent.mt and nFeature_RNA against nCount_RNA with sample-wise correlation annotations. (C) Post-filter per-sample distributions of nFeature_RNA and nCount_RNA. (D) PCA standard-deviation elbow plot used to select the number of principal components. (E-F) Global Louvain clustering shown on t-SNE (E) and UMAP (F) embeddings. (G) Dot plot of canonical cell-type markers across clusters. (H) Feature plots for individual marker genes used for annotation. (I) Stacked violin plot of canonical markers across clusters.

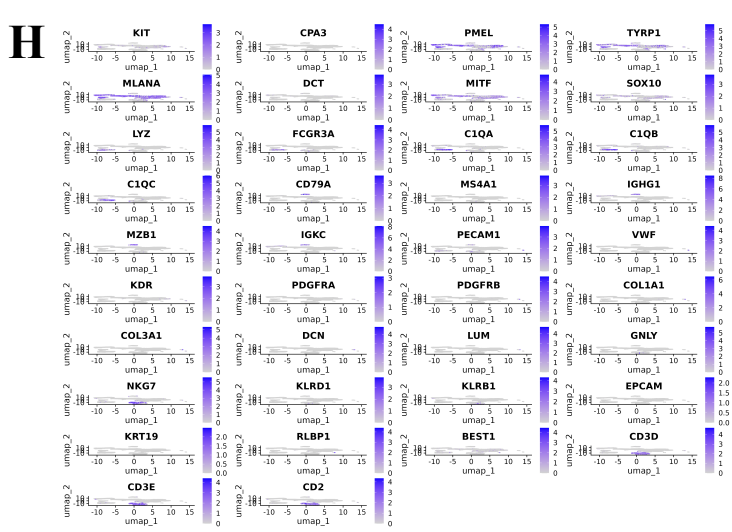


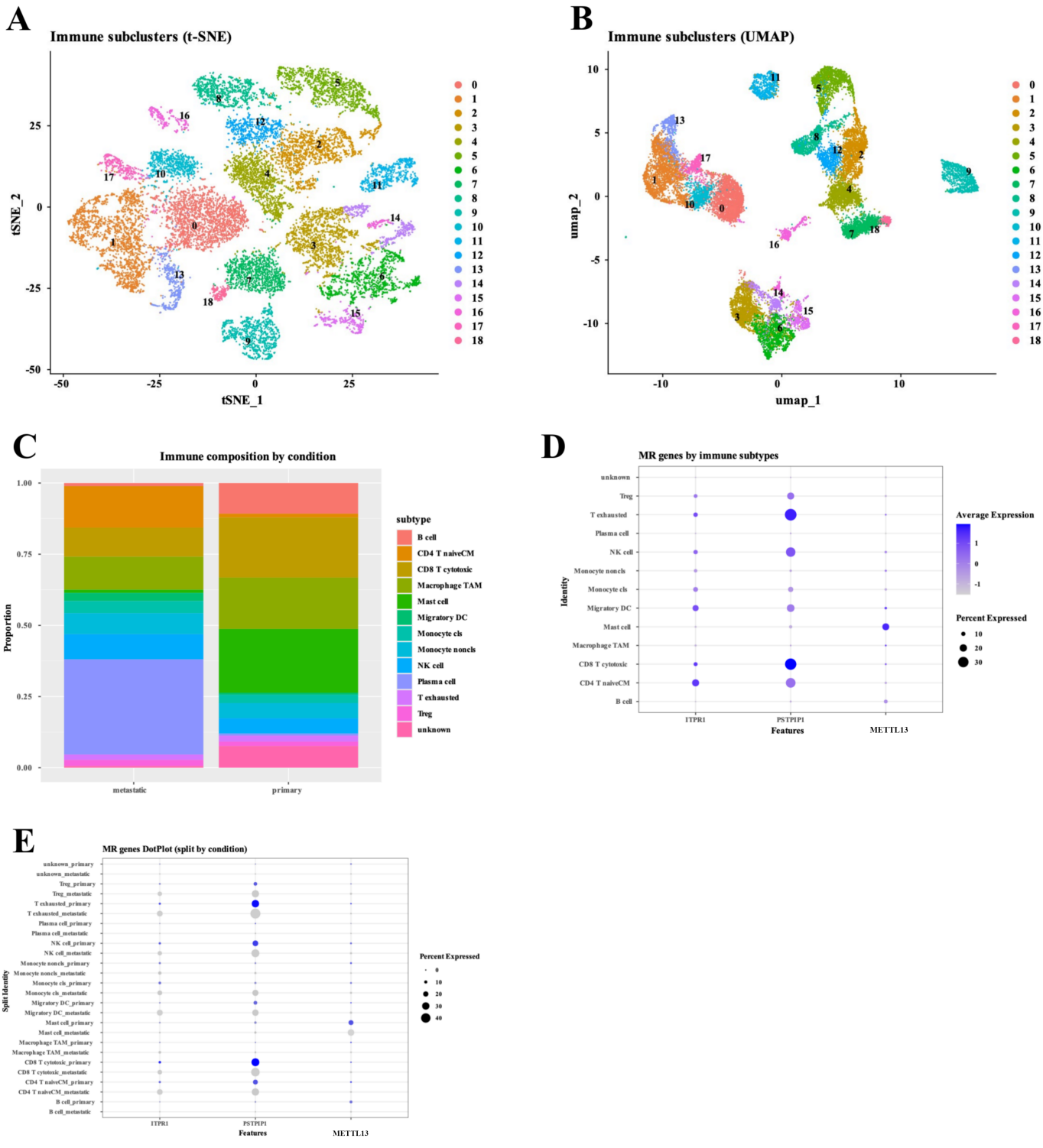



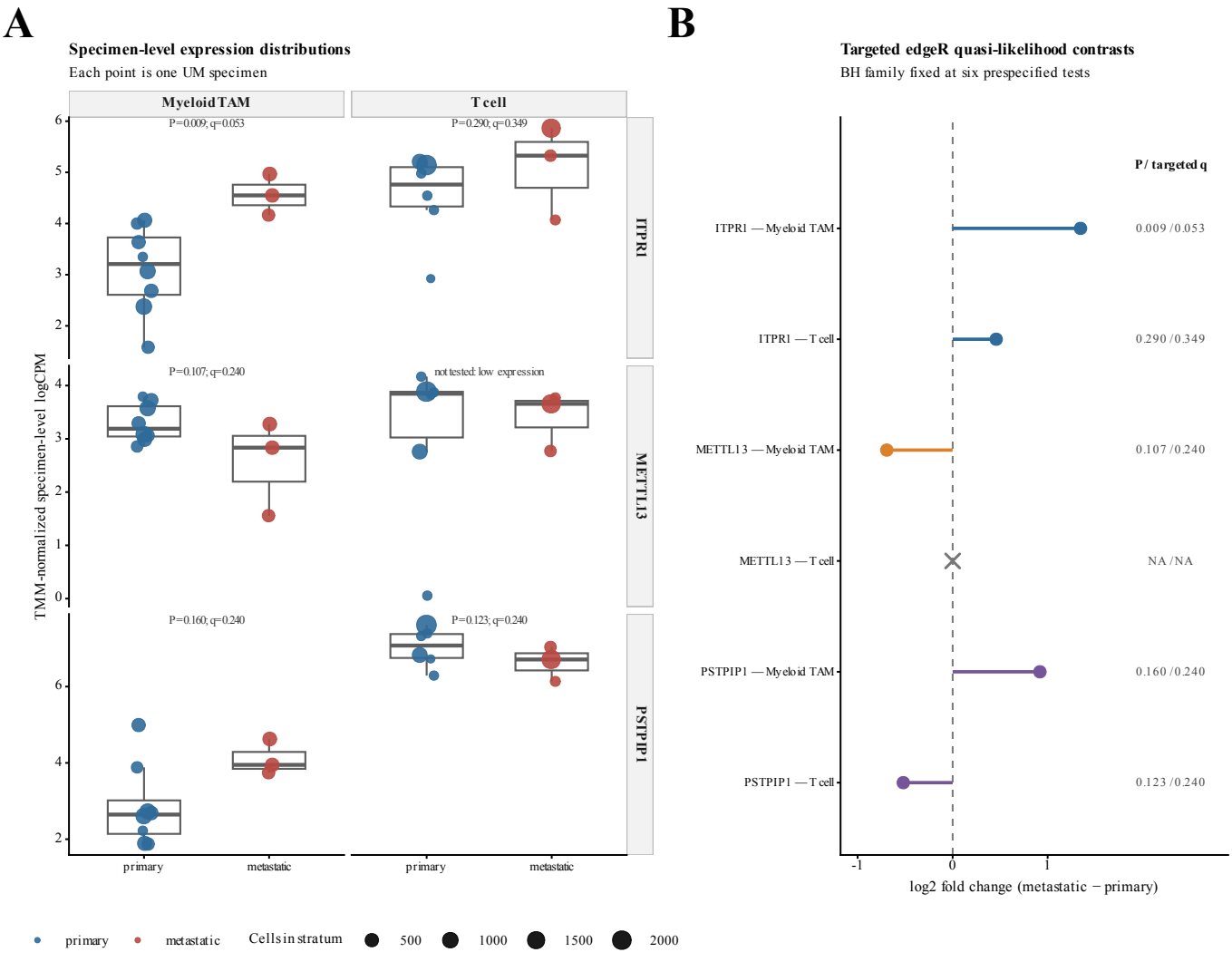
# Figure S5

**Descriptive immune-subset reclustering and candidate-gene expression by subtype and lesion type.**

(A–B) Immune subcluster assignments on t-SNE (A) and UMAP (B) embeddings (Louvain resolution 0.6). (C) Descriptive stacked bar chart of pooled immune-cell proportions in primary and metastatic lesion specimens; this panel does not provide specimen-level estimates or statistical inference. (D) Dot plot of ITPR1, METTL13, and PSTPIP1 expression across annotated immune subtypes. (E) Descriptive dot plot of the three MR-prioritized genes split by immune subtype and lesion type. Cells are pooled within each subtype-by-condition group for visualization; no cell-level P values are interpreted. Formal lesion-type inference is provided by specimen-level pseudobulk in Figure S6.



# Figure S6




Eligibility: ≥10 cells per specimen–cell-type stratum and ≥3 specimens per condition. Myeloid/TAM: 8 primary, 3 metastatic; T cell: 6 primary, 3 metastatic. Five of six contrasts were evaluable; none met targeted BH-FDR < 0.05. This cross-sectional lesion-type comparison does not predict future metastasis.